Chemical Geology 645 (2024) 121899

Contents lists available at ScienceDirect

Chemical Geology

journal homepage: www.elsevier.com/locate/chemgeo

Fossil hydrothermal oceanic systems through *in-situ* B isotopes in ophicarbonates (N. Apennines, Italy)

E. Cannaò [a,*], M. Tiepolo [a], S. Agostini [b], M. Scambelluri [c]

[a] Dipartimento di Scienze della Terra "A. Desio", Università di Milano, Via Botticelli 23, 20133 Milano, Italy
[b] Istituto di Geoscienze e Georisorse, CNR, Via Moruzzi 1, 56124 Pisa, Italy
[c] Dipartimento di Scienze della Terra, Ambiente e Vita, Università di Genova, C.so Europa 26, 16132 Genova, Italy

ARTICLE INFO

Editor: Don Porcelli

Keywords:
Boron isotopes
Ophicarbonates
B cycle
C cycle
Hydrothermal Systems

ABSTRACT

In submarine-hydrothermal systems, fluid-rock interactions play a pivotal role in fostering life on rocky planets. Carbonated-ultramafic rocks (*i.e.,* ophicarbonates) represent an important witness of such environments and their study may provide new insights into hydrothermal processes. Here, we report *in-situ* trace element concentrations and the first *in-situ* boron isotope analyses ($\delta^{11}B$) of serpentines from the Ligurian N. Apennine (Italy) ophicarbonates, which represent non-subducted remnants of Jurassic ultramafic-hosted hydrothermal system. Based on micro-Raman analyses, lizardite is the dominant stable serpentine polymorph in the studied samples, thus constraining the temperature (*T*) of serpentinization below *ca.* 320 °C. By means of U—Pb LA-ICP-MS calcite geochronology, the age of the carbonation event is constrained at 137 ± 3 Ma (2σ, $n = 52$). The increasing inventory of several fluid-mobile elements (*e.g.,* B, Li, As, Sb, Sr, U) associated with the REE budget variability in serpentines from ophicarbonates compared to those in pure serpentinites suggest that physico-chemical changes during the evolution of the hydrothermal system exert a relevant influence on the geochemistry of serpentines. Pure serpentinites, which are considered the protoliths of the ophicarbonates, show positive $\delta^{11}B$ signatures from +15.8 to +35.0‰ ($n = 24$), thus falling in the range of present-day oceanic and forearc serpentinites and ophiolite-derived serpentinites. The $\delta^{11}B$ imprint of serpentines in ophicarbonates clusters at +10.2 ± 2.2‰ (2SD, $n = 57$) and − 5.7 ± 1.5‰ (2SD, $n = 36$). Remarkably, this is the first report of oceanic serpentines showing negative B isotope compositions. The positive $\delta^{11}B$ data likely reflect inheritance from the precursor serpentinite, while the negative $\delta^{11}B$ values are here related to the hydrothermal process(es). We attempt to model how the variation in pH and different $\delta^{11}B$ composition of the hydrothermal vent fluids (+25 and + 8‰) at different *T* (100 and 150 °C) can affect the $\delta^{11}B$ imprint of serpentines. Our results indicate that either pH condition or $\delta^{11}B$ of the hydrothermal vent fluids can shift the $\delta^{11}B$ of serpentines from positive to negative values. Our new trace element and $\delta^{11}B$ data are integrated and discussed with those from the literature to achieve new constraints in the variations and controls on the physical-chemical conditions of fluid-rock interaction during the progressive evolution of long-lived fossil ultramafic-hosted hydrothermal system. Finally, we discuss how subduction processes can potentially modify the B geochemistry of ophicarbonates and the information that we could achieve by studying B isotopes in such high-*P* lithologies to unravel the B- and C-cycles into the Earth's mantle since the onset of modern plate tectonics.

1. Introduction

Oceanic hydrothermal systems are key sites where fluid-rock interactions played a major role in fostering primordial life on Earth (Dodd et al., 2017; Martin et al., 2008) and potentially on other planets and moons (Waite et al., 2017). However, accessing present-day oceanic hydrothermal systems through oceanic expeditions (IODP/ODP; *e.g.*, Kendrick et al., 2022) is challenging and, for this reason, the fossil hydrothermal systems exposed in collisional belts are 3D exposures that improves our understanding of processes occurring in such environments (*e.g.*, Lafay et al., 2017). In this context, the Ligurian Northern (N.) Apennines (Italy) is a key site where a remnant of a seafloor ultramafic-hosted hydrothermal system is exposed (Alt et al., 2018; Barrett and Friedrichsen, 1989; Schwarzenbach et al., 2013; Treves

* Corresponding author.
E-mail address: enrico.cannao@unimi.it (E. Cannaò).

https://doi.org/10.1016/j.chemgeo.2023.121899
Received 11 August 2023; Received in revised form 8 November 2023; Accepted 15 December 2023
Available online 19 December 2023
0009-2541/© 2023 The Authors. Published by Elsevier B.V. This is an open access article under the CC BY-NC-ND license (http://creativecommons.org/licenses/by-nc-nd/4.0/).

et al., 1995; Treves and Harper, 1994). These rocks represent the residue of the Tethyan ocean escaping the Alpine subduction evolution and still record their seafloor-related alteration history (Cortesogno et al., 1975). In the oceanic lithosphere, seawater circulation near the ridge axis generates vent fluids whose chemical variability mainly depends on the type of bedrocks on which they form (*e.g.*, Diehl and Bach, 2020). Carbonates are widespread in both basalt-dominated and ultramafic-hosted hydrothermal systems, forming carbonated mafic-ultramafic rocks (*e.g.*, ophicarbonates), and sulphide mineralization may also occur (Schwarzenbach and Steele-MacInnis, 2020). Being carbonates and sulphides the main products of the hydrothermal vent fluids circulation, most studies have focused on their C-O-S-Sr isotopic signatures (Alt et al., 2012b, 2012a; Schwarzenbach et al., 2018, 2013, 2012). Recently, the attention has also been focused on the trace element signatures of ophiolitic ophicarbonates (Cannaò et al., 2020a; Schwarzenbach et al., 2021), providing new insights into the processes operative in fossil hydrothermal systems. Among the isotopic systematics that still deserve investigation in ophicarbonates, boron (B) is undoubtfully the most promising: serpentine minerals are strongly enriched in B, and their B isotopic signature ($\delta^{11}B$) is a powerful tracer of fluid-rock interactions (*e.g.*, Marschall, 2018). Here we present for the first time a detail *in-situ* $\delta^{11}B$ investigation of non-subducted ophicarbonates from the Ligurian N. Apennines (Italy), providing new constraints on the variations and parameters controlling the physical-chemical conditions of fluid-rock interaction during progressive evolution of a long-lived fossil ultramafic-hosted hydrothermal system. The impact of this rock-type on the B and C subduction cycles is also discussed.

2. Geological background and samples description

In the Ligurian N. Apennine (Italy), oceanic ophicarbonates stratigraphically are atop the serpentinized mantle and underlie the pillow basalts and oceanic sediments (Cortesogno et al., 1980). This rock sequence escaped subduction evolution during the closure of the Tethyan Ocean and the collisional event(s) related to the Alpine orogenesis. Ophicarbonates thus still record the alteration processes that took place on the seafloor (Cortesogno et al., 1975). Based on textural and petrographic features, ophicarbonates are subdivided in ophicarbonates of tectonically and sedimentary derivation, and referred as OCI- and OCII-type, respectively (Lemoine et al., 1987). According to Treves and Harper (1994), the OCI-type ophicarbonates record the tectonic and hydrothermal structures related to tectonic exposure of the oceanic mantle during extensional core-complexes development at slow spreading ridges. The OCII-type ophicarbonates display sub-angular serpentinite/OCI-type clasts embedded in a micrite sedimentary matrix and formed in response to early fragmentation of serpentinitic (and gabbroic) materials in debris flow-like environment (Lemoine et al., 1987). According to Cannaò et al. (2020a), the trace element abundances, as well as the C—O and Sr isotope signatures of these ophicarbonates suggest seawater-rock interactions during Jurassic time. Further geochemical investigations on the serpentinite basement of the N. Apennine ophiolite sequence indicate multiphase water-rock interactions and a complex history of serpentinization during continuous uplift of the ultramafic rocks on the seafloor (Schwarzenbach et al., 2021). Based on field and geochemical evidence, Alt et al. (2018) also proposed that the N. Apennines may represent an evolved high-temperature (*T*) hydrothermal system with black smoker-type venting towards a low-*T* Lost City-type venting. This evolution is also locally preserved in sulphides as documented by their *in-situ* S isotope composition (Schwarzenbach et al., 2018).

Most of the studied samples were already characterized for their bulk and *in-situ* major, minor and trace element concentrations as well as for their bulk C—O and Sr isotope compositions (Cannaò et al., 2020a): one pure serpentinite (sample MNT 15–1), two OCI-type ophicarbonates (samples ISC 13–1 and ZRL 15–3), and two OCII-type ophicarbonates (samples MNT 15–2 and SG 15–4). A new partially serpentinized peridotite (degree of serpentinization ~90%, sample ZRL 15–1) is also considered for this study. Samples with the same label are from the same locality (Fig. 1). The ultramafic protolith of the serpentinites (samples MNT 15–1 and ZRL 15–1) shows medium grain size with isotropic texture suggesting an harzburgite derivation. The static pseudomorphic replacement led to formation of mesh texture made of serpentine + magnetite assemblage on primary mantle olivine and bastite pseudomorph developed after mantle pyroxenes (see Cannaò et al., 2020a). Locally, relicts of clinopyroxene are present in sample ZRL 15–1 (Supplementary Fig. 1). The OCI-type ophicarbonates (samples ISC 13–1 and ZRL 15–3) are characterized by serpentinite clasts of heterogenous sizes and polygonal in shape, with angular to sub-angular edges. Sample ZRL 15–3 shows low degree of carbonation, calcite mainly develops along major fractures and serpentines mostly preserve the texture of the serpentinite *s.s.* protolith. In sample ISC 13–1, the serpentinite clasts are affected by ~20 vol% of carbonation by calcite from the core of the mesh texture and along cleavage of the former pyroxene. Oxidation of the magnetite appears associated with the carbonation process, forming hematite, which is particularly developed along the clasts' boundaries. The OCII-type ophicarbonates display a sedimentary breccia-like texture with clasts consisting of serpentinites or of reworked OCI with typically angular edges and variable grain size (from mm to few hundreds of μm). As for the OCI-type, the dominant mineral assemblage is serpentine + calcite ± talc ± magnetite/hematite. Sample SG 15–4 display minor amount of carbonation and oxidation compared to sample MNT 15–2 showing higher extent of carbonation and oxidation given a characteristic reddish colour to the rock. Both samples are matrix supported made of micritic to sparry calcite.

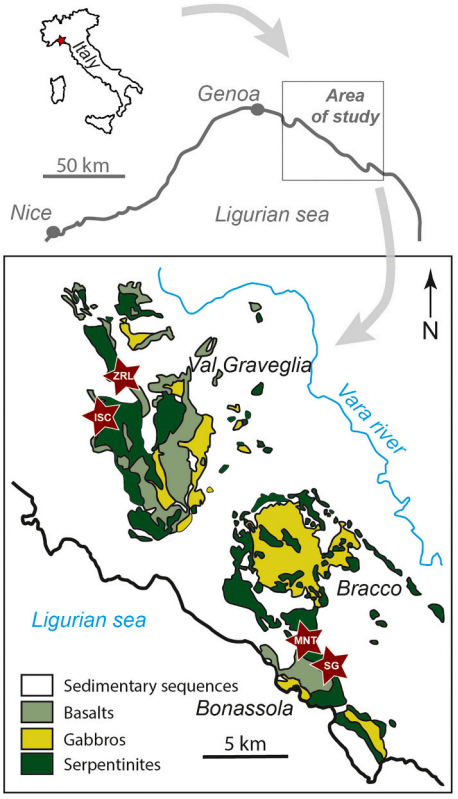

Fig. 1. Simplified geological map of the Internal Liguride domain from the Ligurian N. Apennine ophiolites showing the locations of the investigated samples (red stars; modified from Cannaò et al., 2020a, after Treves and Harper, 1994). (For interpretation of the references to colour in this figure legend, the reader is referred to the web version of this article.)

3. Methods

Identification of the serpentine polymorphs was carried out at the Dipartimento di Scienze della Terra, Ambiente e Vita (University of Genova, Italy) using an XplorRA PLUS Horiba micro-Raman. *In-situ* trace element characterization by laser ablation inductively coupled plasma mass spectrometry (LA-ICP-MS; single-detector quadrupole iCAP RQ, Thermo Fisher Scientific) were performed for selected samples (ZRL15–1, ZRL15–3, and SG15–4) at the Geochemistry, Geochronology and Isotope Geology laboratory of the Dipartimento di Scienze della Terra "A. Desio" (DST – University of Milano, Italy). *In-situ* B isotope compositions of serpentines were measured by laser ablation system (Analyte Excite, Teledyne Photon Machines) coupled with a multi-collector (MC-)ICP-MS (Neptune *XT*, Thermo Fisher Scientific) at the DST (see Appendix A). Bulk B isotope has been determined in solution mode for the pure serpentinite sample MNT 15–1 using a MC-ICP-MS (Neptune *Plus*, Thermo Fisher Scientific) at the IGG-CNR, Pisa (Italy) as described in Agostini et al. (2021). Boron isotope compositions are reported in the standard delta(δ)-notation expressed in permil (‰) relative to the NIST SRM 951 boric acid standard (Catanzaro et al., 1970). Hereafter, the uncertainty of $\delta^{11}B$ is reported as 2 standard deviation (2σ) for average data and as 2 standard error (2SE) for single spot analyses. For ophicarbonate sample SG15–4 (OCII-type), which has suitable U—Pb contents (Cannaò et al., 2020a), we also performed

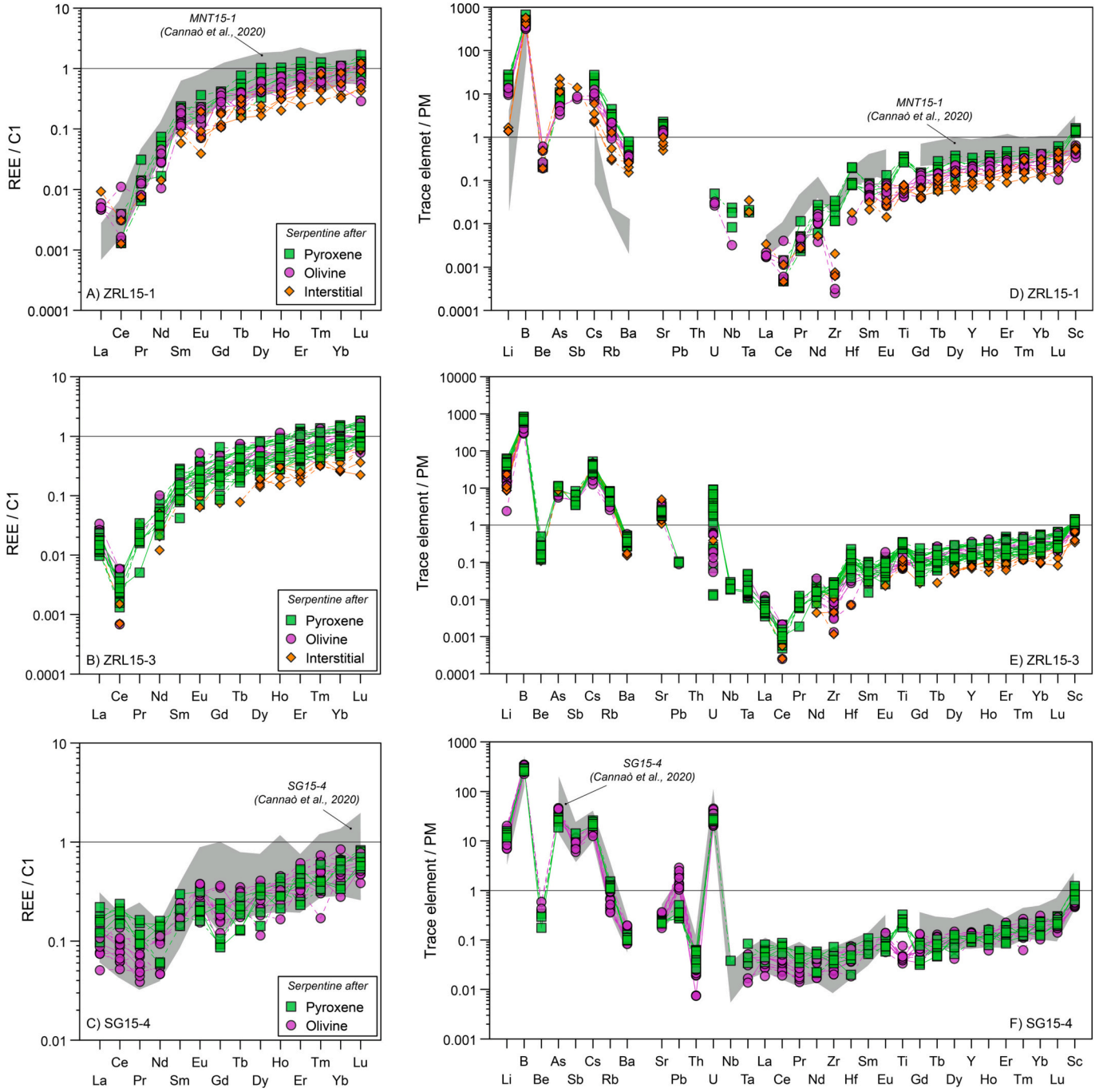

Fig. 2. Chondrite (A-C; C1) REE and primitive mantle (D-F; PM) trace element patterns of serpentinite sample ZRL15–1 (A, D), ophicarbonates samples OCI ZRL15–3 (B, E) and OCII SG15–4 (C—F). Data from pure serpentinite sample MNT15–1 is shown for comparison in A and D as well as data already available for sample SG15–4 (C, F; Cannaò et al., 2020a).

U—Pb calcite geochronology using LA-ICP-MS instrumentation at the DST. Complete analytical details can be found in the Appendix A.

4. Results

4.1. Micro-Raman spectroscopy

Micro-Raman investigations detect strong intensity peaks at *ca.* 226–230, 383–388 and 688–692 cm^{-1} in the vibration region of the alumino-silicate network and main peaks at *ca.* 3684 and 3705 cm^{-1} in the O—H bond stretching region (Appendix A). These features correspond to the low-*T* (below *ca.* 320 °C) lizardite serpentine polymorph (Petriglieri et al., 2015), which is the dominant serpentine polymorph in our samples. However, despite careful petrographic investigations, we cannot completely rule out that, locally, minor amount of chrysotile/antigorite occurs in our samples.

4.2. In-situ trace element concentrations in serpentines

The *in-situ* trace element concentration of serpentine minerals for selected serpentinite (ZRL 15–1) and ophicarbonates (ZRL 15–3 and SG 15–4, OCI- and OCII-type, respectively) are reported in the Supplementary Table 1. The pure serpentinite ZRL 15–1 (Fig. 2A) resembles in trace element composition what reported for the pure serpentinite sample MNT 15–1 (Cannaò et al., 2020a). Rare Earth Element (REE) concentrations are extremely low, and the chondrite normalized patterns (C1, McDonough and Sun, 1995) is characterized by strong depletion in light (L-)REE (down to 0.01 to 0.001/C1) relative to heavy (H-)REE with negligible negative Eu anomaly. Few analyses carried out on former mantle olivine and interstitial mesh texture show variable depletion in Ce. No significant difference in the REE patterns is visible for serpentine sampled in different texture. The REE pattern of the serpentine of the tectonic ophicarbonate OCI-type, sample ZRL15–3, mimics that of the pure serpentinite protolith (sample ZRL 15–1) but with a marked Ce negative anomaly (Fig. 2B), which is typical of the seawater REE pattern (Douville et al., 2002). The REE patterns of serpentines in the sedimentary-derived OCII-type, sample SG 15–4, are more LREE enriched (up to 0.2/C1) than OCI-type and pure serpentinite samples. No evidence of negative Ce anomaly is apparent, whereas a weak positive Eu anomaly is reported for some serpentines replacing both former olivine and pyroxene grains. These trends are compatible with the geochemical features of hydrothermal vent-fluids from several high-*T* hydrothermal fields, such as Rainbow and Logatchev and other MAR fluids (Douville et al., 2002, and references therein). Overall, these geochemical features are consistent with those already published for the same sample (Fig. 2C, Cannaò et al., 2020a). The primitive mantle (PM, McDonough and Sun, 1995) normalized trace element pattern of the pure serpentinite ZRL 15–1 shows high values (>10 times PM) for Li, B, As, Sb and Cs and a slight enrichment also in Rb and Sr (Fig. 2C). Beryllium is above the detection limits only in serpentines replacing former olivine and in some with interstitial texture, otherwise it is always below the PM value. Zirconium and Ti are depleted compared to PM values with significant differences between serpentine replacing former pyroxene and olivine (from 2 to 3–4 times lower than the PM values, respectively), suggesting geochemical inheritance from the precursor mineral. Compared to the trace element concentrations of the pure serpentinite sample MNT 15–1, the ZRL 15–1 serpentines are enriched in several fluid-mobile elements (Li, Be, As, Sb, Cs, Rb, Ba). Noticeably, comparable enrichments in these elements are reported in both the ophicarbonate samples ZRL 15–3 and SG 15–4 (Figs. 2D, E). In particular, the latter shows significant enrichment in Pb and U, as already shown by Cannaò et al. (2020a). In the different samples, B concentrations (Fig. 3) show a positive correlation with Li, Cs and Rb contents. In particular, B, Li and Cs concentrations are higher in serpentines replacing pyroxene compared to those replacing former olivine. Noticeably, a positive correlation between B and U is evident in sample SG 15–4 (Fig. 3F) and between B and As (Fig. 3D) in the ophicarbonate samples. A weak negative correlation is shown between B and Sb (Fig. 3E).

4.3. In-situ elemental and isotopic B characterization of serpentine

In-situ B isotope composition of serpentine in serpentinites and ophicarbonates are reported in Table 1 and presented in Fig. 4. Serpentinites MNT 15–1 and ZRL 15–1 are differently enriched in B, from 28.6 ± 3.2 to 134 ± 57 ppm, and show a distinct *in-situ* $\delta^{11}B$ signature with mean compositions of +32.0 ± 2.4‰ ($n = 12$) and + 16.8 ± 2.7‰ (n = 12), respectively (Fig. 4). Noticeably, the *in-situ* results for the sample MNT 15–1 closely approach the bulk $\delta^{11}B$ value of +35.34 ± 0.15‰. The less carbonated OCI-type ophicarbonate (sample ZRL 15–3) is characterized by similar [B] of the ZRL protolith (190 ± 79 ppm) but shows lower $\delta^{11}B$ values averaging at +10.4 ± 2.0‰ ($n = 53$). The more carbonated and oxidized OCI-type ophicarbonate (sample ISC13–1) shows slightly lower [B] of 78.1 ± 16.8 ppm and $\delta^{11}B$ of −4.8 ± 1.0‰ ($n = 8$). The less and more oxidized OCII-type ophicarbonates (samples SG 15–4 and MNT 15–2, respectively) have [B] in between the two OCI values (from 68 to 178 ppm) and $\delta^{11}B$ of −6.0 ± 1.1‰ ($n = 28$) and + 8.5 ± 1.8‰ ($n = 4$), respectively. Remarkably, the negative $\delta^{11}B$ signatures shown by samples ISC 13–1 and SG 15–4 are the first negative values reported so far for oceanic-derived ultramafic rocks. In ZRL samples and few clasts in SG 15–4, serpentines replacing olivine are characterized by slightly higher $\delta^{11}B$ values with respect to serpentines replacing pyroxene (*ca.* +2 to +4‰), $\delta^{11}B$ variation along rim-core-rim profiles are also documented (Figs. 5–7; Supplementary Figs. 2, 3). Boron isotope composition of ophicarbonates ZRL 15–3 (OCI-type) and SG 15–4 (OCII-type) show negative correlation with Li content and sample SG 15–4 also shows a weak negative correlation between $\delta^{11}B$ imprint and U content of the serpentine minerals (Fig. 8).

4.4. U—Pb geochronology of calcite

A U—Pb lower-intercept age of 137 ± 3 Ma (2σ, $n = 52$; Fig. 9) was obtained for the carbonates of the OCII-type sample SG 15–4 (Supplementary Table 2) and is the first geochronological date available for the fossil hydrothermal system of Ligurian N. Apennine, so far. This date is younger than the age range (*ca.* 165–161 Ma) for the MORB intrusions in the peridotites of the Internal Liguride ophiolites (Tribuzio et al., 2016, and reference therein). Carbonates of the OCII-type sample SG 15–4 are also significantly younger than the igneous activity occurred during the late stages of rifting and represented by the plagiogranite from the Bracco-Val Graveglia Unit in the N. Apennines, dated at 153.3 ± 1.0 Ma (Borsi et al., 1996). The age of *ca.* 137 Ma for the N. Apennine hydrothermal system agrees with the U—Pb age of 144 ± 14 Ma documented for calcite veins from the paleo-detachment plane from the Platta nappe in the Alps, interpreted as the root zone of a fossil ultramafic-hosted black smokers-like hydrothermal system (Coltat et al., 2019). Overall, this age also agrees with that of the stratigraphic base of the sedimentary sequence placed in direct contact with the serpentinite/ophicarbonate basement (*e.g.*, Perilli and Nannini, 1997).

5. Discussion

5.1. On the B isotope variability in pure serpentinites

The B isotope systematic is strongly sensitive to changes in pH and *T* of the system, making oceanic serpentinites a heterogenous B reservoir with variable $\delta^{11}B$ signatures (*e.g.*, Boschi et al., 2008). The B isotope composition of pure (*i.e.,* non-carbonated) serpentinites from the Ligurian N. Apennine falls within the range of present-day oceanic and forearc serpentinites and serpentinites from ophiolite complexes (Fig. 4; Marschall, 2018, and references therein). The $^{87}Sr/^{86}Sr$ ratio of the pure serpentinite sample MNT 15–1 (0.7069, Cannaò et al., 2020a) is close to

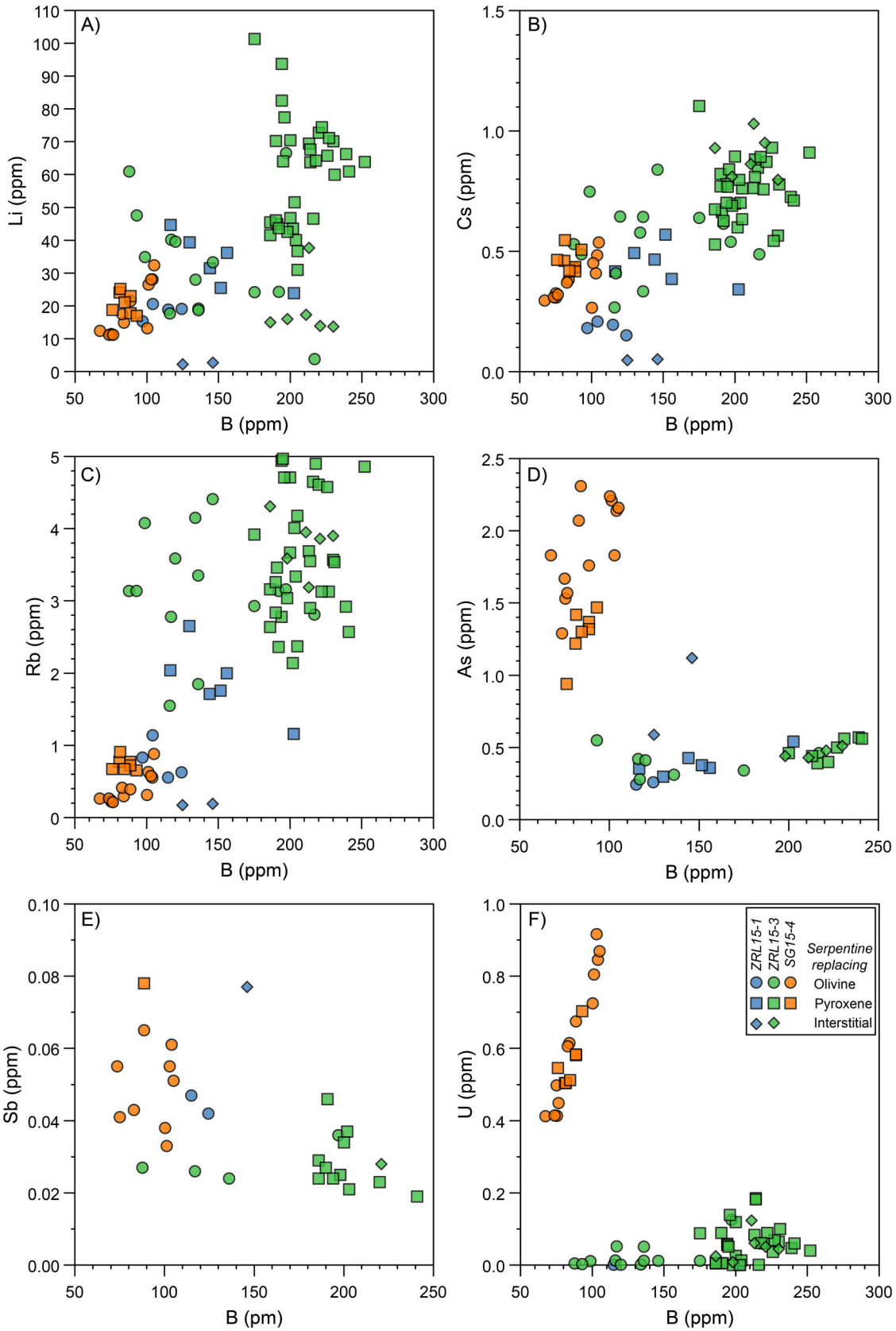

Fig. 3. Variability of B with key fluid-mobile and redox elements: Li (A), Cs (B), Rb (C), As (D), Sb (E), U (F).

Table 1
In-situ B isotope composition of serpentines and B concentrations.

Lithology	Sample	B (ppm)$_{LA-ICP-MS}$	B (ppm)*	δ^{11}B (‰)	2SE (‰)
Pure serpentinite	MNT15–1	*Not determined*	25.8	+32.5	0.5
			27.7	+32.8	0.7
			30.5	+31.0	0.6
			30.3	+31.1	0.6
			27.7	+32.8	0.5
			28.1	+35.0	0.4
			29.4	+33.3	0.6
			29.5	+33.7	0.5
			27.2	+31.0	0.6
			26.7	+31.5	0.7
			29.9	+32.1	0.6
			30.1	+33.1	0.5
	average		*28.6*	*+32.5*	
	2σ		*3.2*	*2.4*	
Pure serpentinite	**ZRL15–1**	144	135	+16.7	0.3
		130	144	+16.5	0.4
		117	124	+15.9	0.3
		156	162	+16.0	0.3
		203	182	+15.8	0.3
		152	136	+15.8	0.3
		104	99.0	+17.0	0.3
		97	93.2	+17.0	0.4
		124	113	+19.6	0.4
		115	116	+19.5	0.5
		125	121	+15.8	0.3
		146	156	+16.5	0.3
	average	*134*	*132*	*+16.8*	
	2σ	*57*	*53*	*2.7*	
OCI-type ophicarbonate	**ZRL15–3**	134	126	+11.0	0.4
		192	171	+10.5	0.3
		146	146	+11.7	0.3
		175	155	+11.4	0.3
		136	129	+10.6	0.3
		117	130	+11.2	0.3
		116	122	+11.2	0.3
		136	125	+11.1	0.3
		98.7	88.8	+11.1	0.3
		87.6	97.3	+11.4	0.3
		92.9	106	+11.7	0.3
		120	131	+10.5	0.3
		217	217	+9.9	0.2
		197	198	+9.2	0.3
		200	174	+10.4	0.3
		191	193	+10.7	0.3
		186	166	+10.9	0.2
		186	232	+10.1	0.3
		204	217	+10.0	0.3
		190	200	+10.4	0.3
		202	201	+10.3	0.3
		205	224	+10.6	0.3
		198	171	+10.6	0.2
		192	197	+10.6	0.2
		205	248	+10.7	0.3
		216	224	+10.7	0.2
		203	191	+10.5	0.2
		175	156	+9.2	0.3
		213	213	+9.5	0.2
		239	213	+8.9	0.2
		230	219	+9.7	0.3
		220	244	+9.1	0.3
		194	203	+8.8	0.2
		231	213	+9.0	0.3
		227	205	+9.1	0.3
		194	215	+8.3	0.2
		222	253	+9.4	0.3
		214	234	+10.0	0.3
		190	190	+10.5	0.4
		214	216	+9.8	0.3
		241	209	+9.9	0.3
		226	228	+9.3	0.3
		195	174	+9.5	0.2
		200	250	+8.4	0.3
		252	268	+9.9	0.2
		218	230	+10.0	0.2
		196	195	+9.8	0.3
		198	216	+11.5	0.4
		186	160	+12.0	0.4
		230	236	+12.1	0.5
		221	268	+11.5	0.3
		211	218	+12.7	0.2
		213	185	+12.0	0.3
	average	*190*	*192*	*+10.4*	
	2σ	*79*	*88*	*2.0*	
OCI-type ophicarbonate	**ISC13–1**	*Not determined*	80.6	−5.1	0.5
			80.8	−5.4	0.5
			82.6	−5.1	0.4
			69.2	−5.2	0.7
			66.0	−3.9	0.4
			79.4	−4.7	0.6
			73.7	−4.4	0.6
			92.8	−4.5	0.4
	average		*78.1*	*−4.8*	
	2σ		*16.8*	*1.0*	
OCII-type ophicarbonate	**MNT15–2**	*Not determined*	144	+8.3	0.6
			178	+8.9	0.6
			150	+7.3	0.5
			151	+9.4	0.7
	average		*155*	*+8.5*	
	2σ		*30*	*1.8*	
OCII-type ophicarbonate	**SG15–4**	*Not determined*	77.3	−5.8	0.4
			76.2	−6.1	0.4
			88.7	−5.7	0.4
			36.1	−5.6	0.4
			30.4	−5.7	0.5
			23.8	−5.0	0.5
			60.9	−6.8	0.4
			75.5	−7.0	0.4
		83.9	86.4	−5.3	0.5
		82.8	70.4	−6.1	0.5
		67.3	65.3	−5.4	0.4
		75.1	69.9	−5.5	0.5
		88.5	92.1	−5.7	0.4
		75.3	78.3	−5.3	0.5
		73.6	64.8	−6.0	0.5
		76.5	83.3	−5.6	0.5
		104	106	−6.3	0.5
		101	93.1	−6.5	0.5
		103	116	−7.3	0.6
		105	89.4	−5.1	0.5
		100	96.2	−6.4	0.4
		81.0	79.4	−6.0	0.5
		81.4	74.1	−6.2	0.5
		88.6	93.9	−5.5	0.4
		92.9	97.6	−5.9	0.5
		88.5	94.7	−6.4	0.4
		84.5	92.9	−6.1	0.4
		76.1	67.0	−6.4	0.4
	average	*86.5*	*77.9*	*−6.0*	
	2σ	*22.8*	*42.8*	*1.1*	

*B content estimated with LA-MC-ICP-MS.

that of Jurassic seawater (~0.7070; McArthur et al., 2001) and constrains the serpentinization environment to the Tethyan seafloor (Cannaò et al., 2020a). The Early Cretaceous U—Pb age of 137 ± 3 Ma (Fig. 9) obtained from a late calcite vein from the OCII-type ophicarbonate (sample SG 15–4) suggests that carbonation took place during alteration of mantle rocks in a fossil hydrothermal system, well after the opening of the Jurassic Tethys (dated at *ca.* 160 Ma; see Tribuzio et al., 2016 and references therein). This OCII-type ophicarbonate sample lies atop the ophiolite ultramafic sequence (Treves et al., 1995), suggesting that seafloor exposure occurred in relation to detachment faulting (Alt

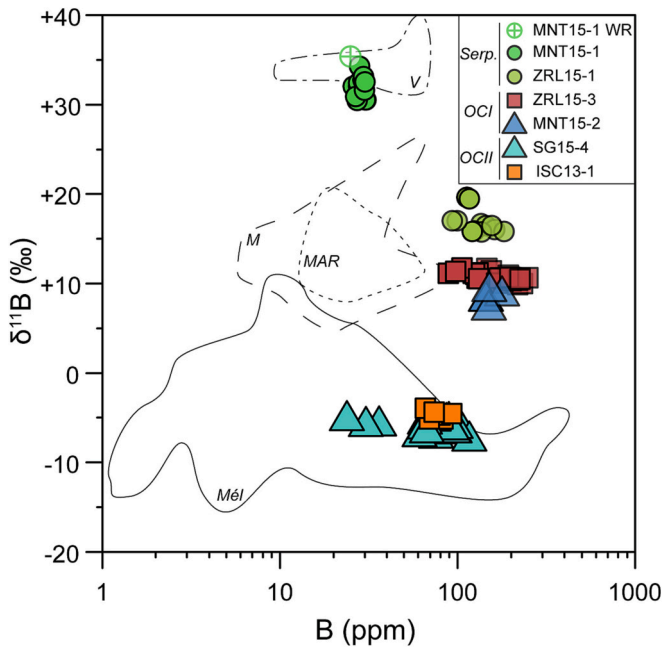

Fig. 4. *In-situ* B (ppm) *vs.* δ^{11}B (‰) of investigated samples compared with reference data for serpentinites: Mid-Atlantic Ridge (MAR; Boschi et al., 2008), ODP LEG 209 (V: Vils et al., 2009), Mariana forearc (M: Benton et al., 2001) and mélange settings (Mél: Martin et al., 2016). For sample MNT15–1 its whole rock (WR) data is also shown. Boron concentrations are semiquantitative estimated by LA-MC-ICP-MS (see Appendix A).

et al., 2018). Based on the δ^{18}O isotope composition of serpentinites from the same area (Schwarzenbach et al., 2021, 2013), the serpentinization process occurred at *T* between 150 and 240 °C. Within this *T* range, oceanic serpentinization of mantle rocks by seawater (δ^{11}B ≈ +39.6‰, pH ≈ 8.2) produces serpentinites with positive δ^{11}B signatures ranging from +17 to +23‰ (*e.g.*, Boschi et al., 2008), values that are consistent with those of the partially serpentinized sample ZRL 15–1. The high δ^{11}B value of +35 ‰ reported for the MNT 15–1 serpentinite either requires more alkaline conditions of the alteration fluids (pH value up to 9) (Boschi et al., 2008; Vils et al., 2009) or higher *T* of alteration, still within the low-*T* lizardite stability field (below *ca.* 320 °C; *e.g.*, Schwartz et al., 2013). In this context, *in-situ* S isotope data support that, at least locally, high-*T* fluids (in the range of up to 350 °C) infiltrated serpentinites before mantle rock exposure on the seafloor (Schwarzenbach et al., 2018). Notably, an increase in fluid pH during serpentinization can also change the δ^{11}B rock composition upon reaction (Vils et al., 2009). The REE and incompatible element inventory of ZRL 15–1 and MNT 15–1 samples (Figs. 2A-D) also indicate a different evolution during seafloor serpentinization, consistent with the B isotope results. However, a conclusive explanation for the discrepancy in the δ^{11}B composition of these two representative pure serpentinite samples requires further investigations (*e.g.*, δ^{18}O-δD data), that are beyond the purpose of this work. Nevertheless, for sample ZRL 15–1, our *in-situ* results reveal different δ^{11}B signatures of serpentines replacing former olivine and pyroxene (Fig. 5) and provide evidence of the evolving fluids during peridotite serpentinization at the sample scale. Since B uptake and B isotope fractionation in hydrous minerals is highly sensitive to *T* (Seyfried and Dibble, 1980; Vils et al., 2009), the [B] and δ^{11}B variability in serpentine shown in Fig. 5 may reflect *T* variation during mantle emplacement and cooling at the ocean floor. We propose that in sample ZRL 15–1, olivine was hydrated before pyroxene due to its high dissolution rates (Mével, 2003), as also suggested by petrographic observation showing relict of mantle pyroxene and the lack of primary mantle olivine. With the progress of serpentinization reactions, hydration of pyroxene takes place with further uptake of B (Seyfried and Dibble, 1980) coupled with increasing B isotope fractionation due to the preferential ^{11}B retention in the fluid phase (*e.g.*, Boschi et al., 2008). Support to this scenario is also the Li enrichment of serpentines replacing pyroxene relative to those replacing olivine (Fig. 3A), thus reinforcing the scenario of low-*T* evolution during pyroxene alteration (Seyfried et al., 1984). Inheritance of the Li inventory from precursor mantle minerals is unlikely due to the low Li content in primary mantle olivine and pyroxenes (Decitre et al., 2002). Although further detailed *in-situ* information are needed to better unravel the geochemical behaviour of B isotope during serpentinization progress at the micro-scale, our results show the heterogeneous and variable δ^{11}B signatures affecting exposed mantle peridotites before carbonation processes leading to development of ophicarbonates.

5.2. *On the B isotope variability in ophicarbonates*

5.2.1. *δ^{11}B inheritance from the serpentinite precursors*

Understanding the geochemical variability of pure serpentinites provides a basis for unravelling the more complex B isotope behaviour in ophicarbonate systems, where vent fluid end-members may have extremely different chemical features (Diehl and Bach, 2020, and references therein). When compared with the pure serpentinite ZRL 15–1 (Fig. 4), the variably carbonated and oxidized samples ZRL 15–3 (OCI-type) and MNT 15–2 (OCII-type) display slightly lower but still comparable and positive δ^{11}B signatures (Table 1). In particular, the serpentine pseudomorphs after olivine and pyroxene in the ophicarbonates ZRL 15–3 cluster at different δ^{11}B values with a gap of approximately 1‰ (Fig. 6), and this δ^{11}B variability has rim-to-rim systematic trends in former pyroxene and olivine sites. These B isotope compositions, together with their seawater-like REE patterns (Fig. 2B), suggest large inheritance from the serpentinite precursor and that limited geochemical overprinting occurred during the hydrothermal history related to carbonation episode(s). In contrast, samples ISC 13–1 and SG 15–4 (OCI- and OCII-type ophicarbonate, respectively) show systematically lower and negative δ^{11}B compositions down to approximately −6‰ (Fig. 4). Comparably negative δ^{11}B values in serpentines have been so far attributed only to wedge-derived serpentinites flushed by deep slab-derived fluids (Martin et al., 2016). Based on the halogen concentrations, especially the Br/Cl and I/Cl ratios of serpentinites, Kendrick et al. (2013) suggested that sedimentary marine pore fluids were involved in the serpentinization of the Ligurian N. Apennine (Internal Ligurides) ultramafic rocks. However, present-day marine pore fluids are commonly characterized by high δ^{11}B signatures, within ±10‰ the present-day seawater value of ~ +39.6‰ (Kopf et al., 2000; Spivack and You, 1997; You et al., 1995). Therefore, the interaction with such a ^{11}B-rich reservoir cannot produce serpentinites with negative δ^{11}B imprint. According to Schwarzenbach et al. (2021), some serpentinites from the N. Apennine show high radiogenic ^{87}Sr/^{86}Sr ratios, suggesting that serpentinization occurred by interaction with fluids with hybrid composition having seawater and continental sediments as major end-members. Although still unknown, the δ^{11}B imprint of these serpentinites should be lower than that of the pure seawater end-member trending towards lower and (perhaps) negative values typical of continental sediments (Trumbull and Slack, 2018). The possibility that the negative δ^{11}B documented in some of our serpentinite clasts in the OCI- and OCII-type ophicarbonates may derive from this type of protolith cannot be ruled out. Remarkably, pure serpentinites from oceanic environment with negative δ^{11}B signatures, however, still must be documented in the Ligurian N. Apennine and worldwide.

5.2.2. *δ^{11}B re-equilibration with hydrothermal vent fluids*

Textural evidence indicates that in the studied ophicarbonate samples carbonation postdates serpentinization of the mantle precursors (Cannaò et al., 2020a; Schwarzenbach et al., 2013; Treves et al., 1995). However, the initial geochemical signatures of serpentinites might not be preserved by the serpentine clasts of ophicarbonates. Hereafter, we

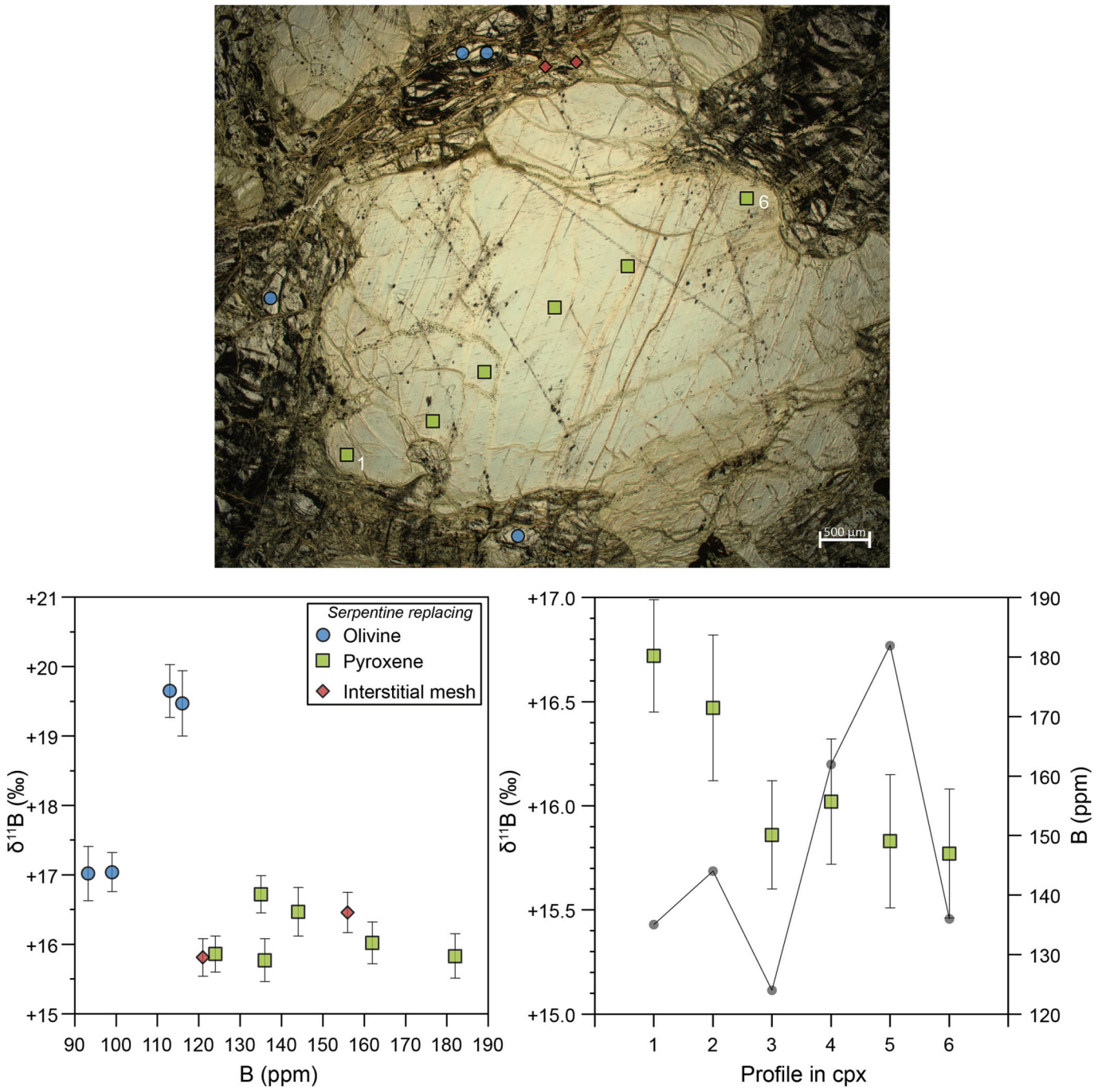

Fig. 5. *In-situ* B (ppm) and δ^{11}B (‰) variability in serpentines replacing former olivine and pyroxene grains in pure serpentinite ZRL15–1.

explore the possibility that the negative B isotopic signature shown by sample SG 15–4 (and sample ISC 13–1) is unlikely to be inherited from a precursor serpentinite with an unusual negative B isotope composition. Instead, we propose a geochemical re-equilibration of the serpentinite with hydrothermal vent fluids. The comparison between the REE pattern of sample SG 15–4 (Fig. 2C) and that of the pure serpentinites (both samples ZRL 15–1 and MNT 15–1, Figs. 2A, B) reveals interaction with fluids with different composition. While the REE patterns of the pure serpentinites show evidence of seawater-like derivation (*i.e.,* negative Ce anomaly), the REE patterns of the sample SG15–4 mostly reflect vent fluids composition sourced from high-*T* hydrothermal fields (*i.e.,* lack of negative Ce anomaly, higher LREE and slightly positive Eu anomaly), such as Rainbow and Logatchev and other MAR fluids (Douville et al., 2002, and references therein). The influx of vent-derived fluids from high-*T* hydrothermal fields is further supported by variations in other fluid-mobile and redox-sensitive elements, such as As, Sb and U (Figs. 3D-F) suggesting a strong influence of redox conditions (Lafay et al., 2016) and high fluid/rock ratios during the hydrothermal activity (Andreani et al., 2014) recorded by sample SG 15–4. The $^{87}Sr/^{86}Sr$ ratios of the N. Apennine ophicarbonates characterized by negative δ^{11}B range from 0.7065 to 0.7057, values from slightly to significantly lower than the Jurassic-Cretaceous seawater (*ca.* 0.7070, McArthur et al., 2001). This less-radiogenic signatures support a higher influence of the vent fluid end-members, dominated by seawater equilibrated with gabbroic lithologies (Schwarzenbach et al., 2021). In particular, the low Sr radiogenic imprint of the less carbonates OCII-type sample SG 15–4 of 0.7057 clearly indicates the lack of sedimentary-signature (*i.e.,* radiogenic Sr ratio), thus suggesting that the negative δ^{11}B of −6‰ cannot be

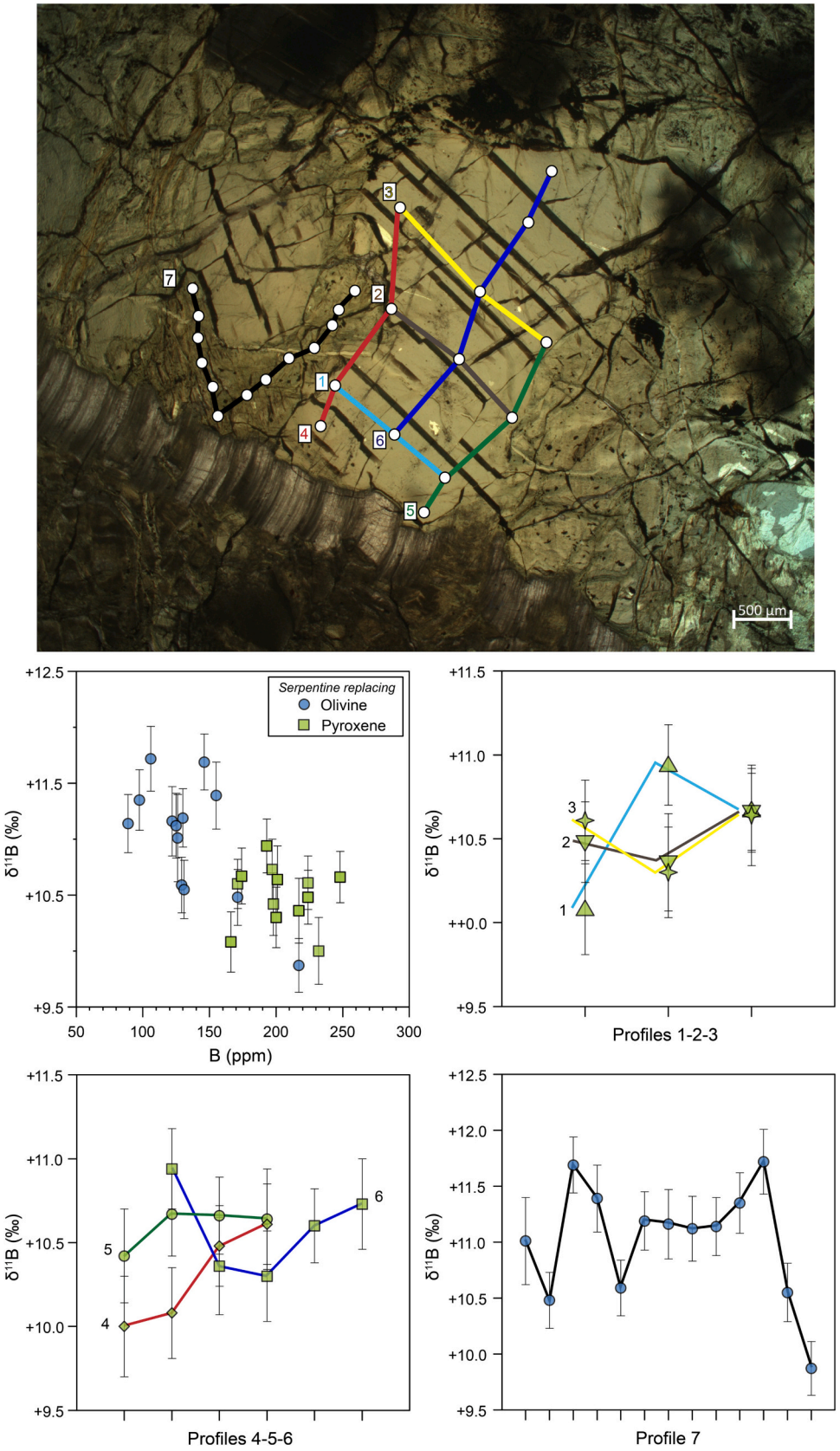

Fig. 6. *In-situ* B (ppm) and $\delta^{11}B$ (‰) variability in serpentines replacing former olivine and pyroxene grains along different profiles in ophicarbonate OCI, sample ZRL15–3.

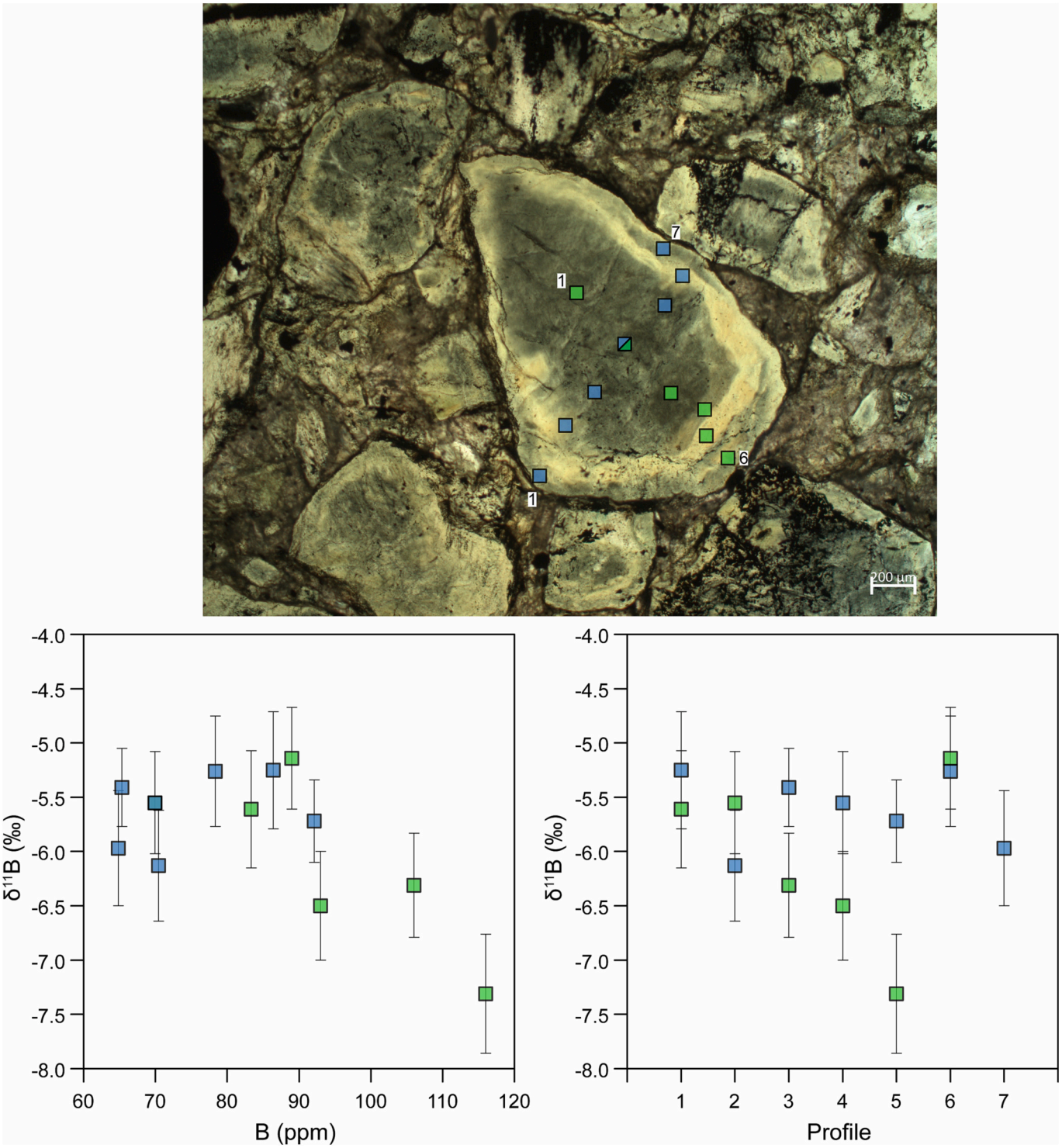

Fig. 7. *In-situ* B (ppm) and δ^{11}B (‰) variability along two cross-cutting profiles within a serpentinite clast from ophicarbonate OCII, sample SG15–4.

related to inheritance of serpentinite protoliths with sedimentary-like Sr isotope composition. We propose that the B isotope signature of the serpentines may also have been affected by the hydrothermal activity. Unfortunately, the chemical composition of the hydrothermal vent fluids at the origin of the Ligurian N. Apennine ophicarbonates is unknown, hence the present-day hydrothermal vents (Diehl and Bach, 2020, and references therein) are used as analogous to gain information into the behaviour of B isotopes of this fossil hydrothermal system (see Supplementary Fig. 4). Based on the δ^{18}O composition of carbonates in the Ligurian N. Apennine ophicarbonates the estimated *T* of carbonation decreases from 150 to 50 °C for earlier and tardive veins, respectively (Cannaò et al., 2020a; Schwarzenbach et al., 2013). Boron concentration in low-*T* hydrothermal fluids (*e.g.,* Lost City) is approximately 5 to 8 times lower than in high-*T* vent fluids (*e.g.,* Rainbow and Logatchev), consistent with the uptake of B in the mineral phases at low-*T* (Seyfried and Dibble, 1980). Direct measurements of the δ^{11}B signature in peridotite-hosted hydrothermal vent fluids are not available. Nevertheless, the δ^{11}B for Lost City, for instance, was indirectly estimated to vary between +25 and +30‰ (Foustoukos et al., 2008). In contrast, data for low-*T* basalt-hosted vent fluids show strongly positive δ^{11}B

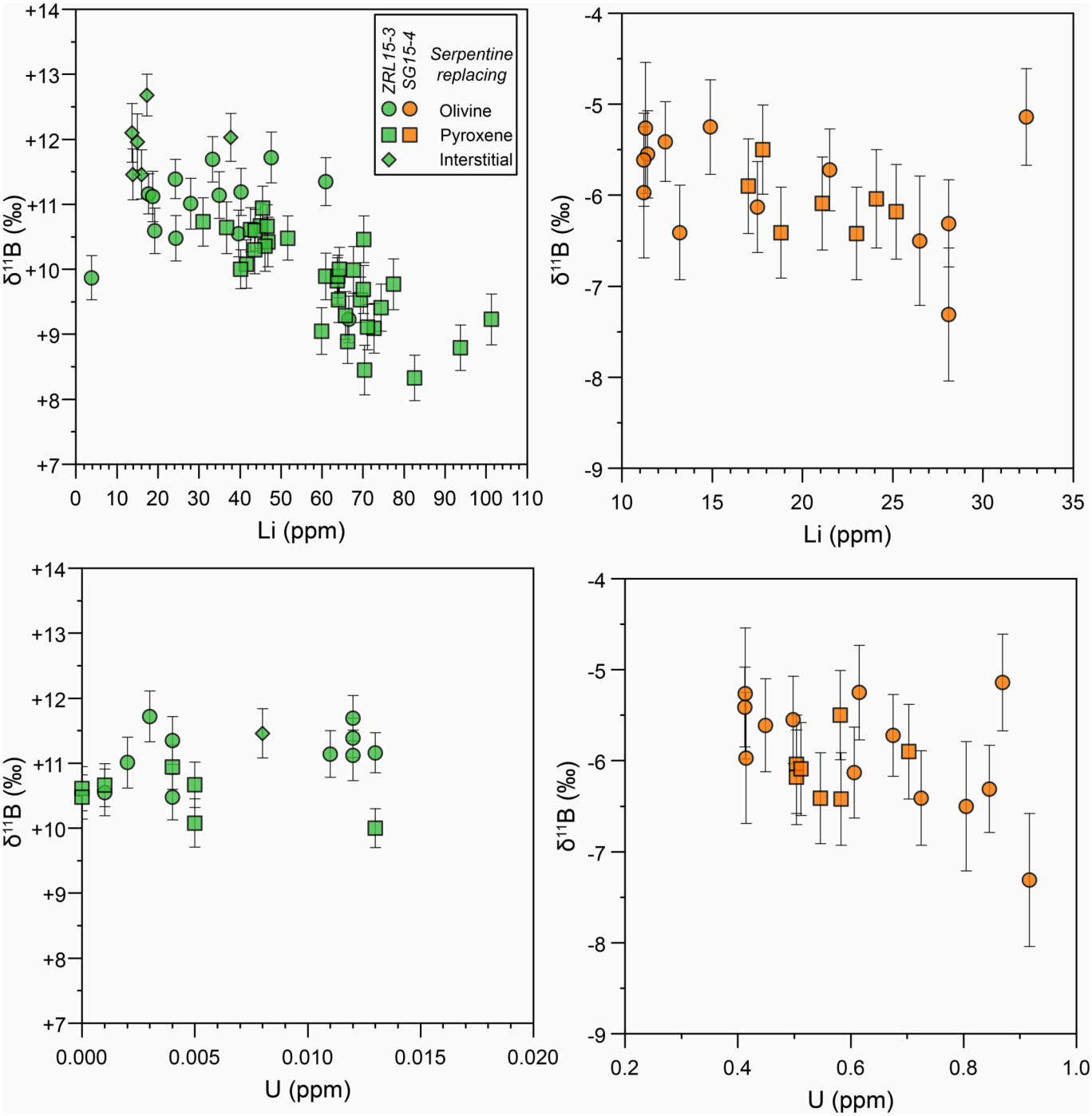

Fig. 8. Correlation between *in-situ* $\delta^{11}B$ (‰) and Li (ppm) and U (ppm) in serpentines replacing former pyroxene and olivine in ophicarbonates ZRL15–3 (OCI) and SG15–4 (OCII).

signatures at acidic conditions (up to +35‰), whereas lower, but still positive, $\delta^{11}B$ values are reported in alkaline ones (down to +10‰). This behaviour likely reflects the effect of pH on the fractionation of B isotopes between fluid and minerals. If present-day hydrothermal vents are used as analogous, the pH of peridotite-hosted vent fluids would range from 5.5 in the Von Damm (Mid-Cayman Rise) to 11.0 in the Lost City (Mid-Atlantic Ridge) vent fields in relation to change in *T* from 150 to 50 °C, respectively – *i.e.,* approaching the *T* estimated for the Ligurian N. Apennine ophicarbonates (Cannaò et al., 2020a; Schwarzenbach et al., 2013). Notably, at low pH conditions almost all B is speciated as $B(OH)_3$, limiting the incorporation of ^{11}B into tetrahedrally coordinated phases, such as serpentine, and potentially shifting the $\delta^{11}B$ of serpentine to lower, and paraphs negative, values. To test if the negative B isotopic signature of −6‰ shown by samples SG 15–4 and ISC 13–1 was acquired during interaction with hydrothermal vent fluids, we attempt to model how variations in pH can affect the $\delta^{11}B$ of serpentines. We considered hydrothermal vent fluids with different $\delta^{11}B$ signatures: i) comparable to those of the Lost City (+25‰, Foustoukos et al., 2008), ii) at the lower end of the present-day $\delta^{11}B$ values for hydrothermal vent fluids (equal to +8‰, see Supplementary Fig. 5). Fig. 10A and B report the relative abundance of major aqueous B species ($B(OH)_3$ and $B(OH)_4^-$) as a function of pH at *P-T* conditions (100–150 °C and 500 bars) estimated for the carbonate precipitation in the N. Apennine hydrothermal system (*e.g.*, Cannaò et al., 2020a). At 100 °C, the pH neutrality is at 6.2, and

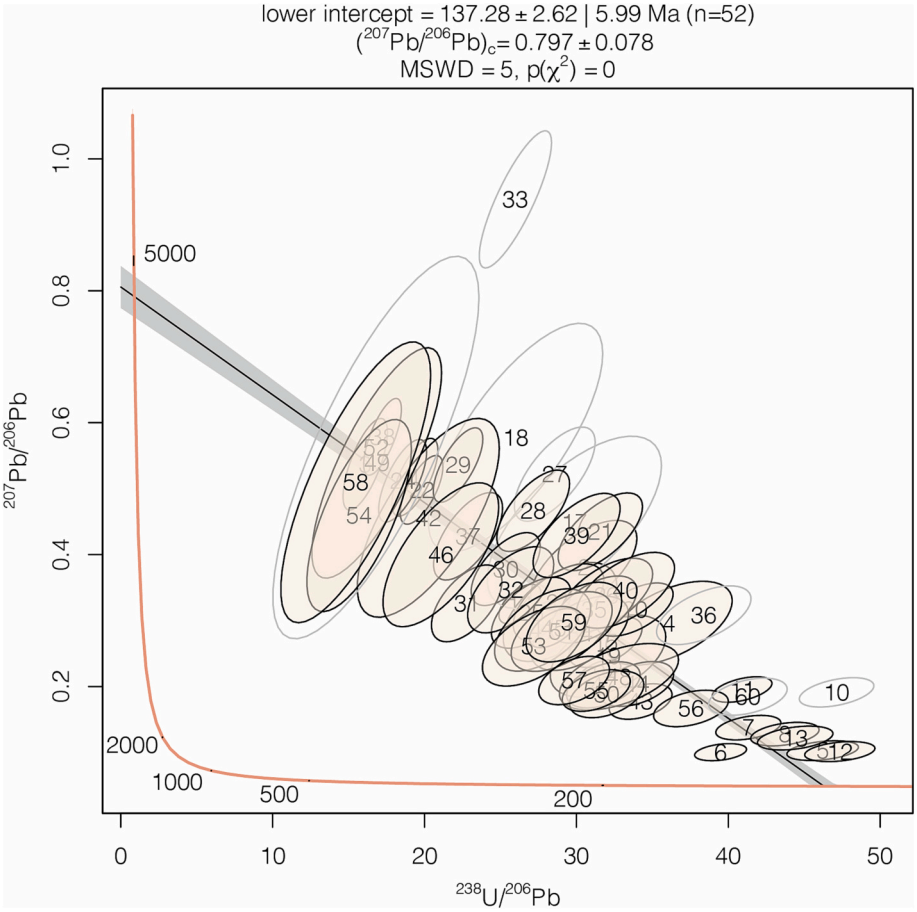

Fig. 9. Tera-Wasserburg plot of calcites from sample SG15–4 (OCII). Empty ellipses are data omitted from the calculation. Isochron calculation were performed using IsoplotR (Vermeesch, 2018).

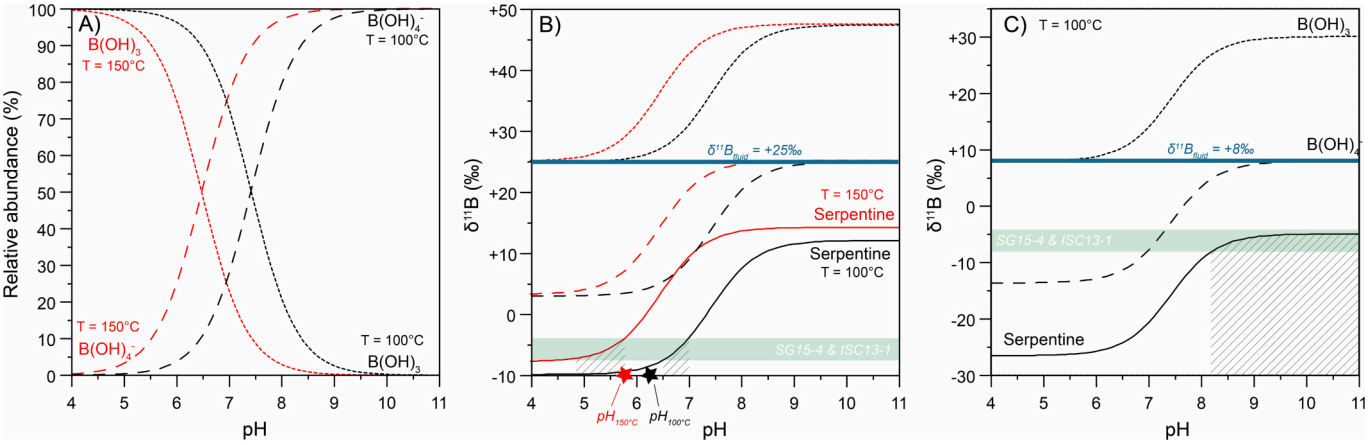

Fig. 10. (A) Boron speciation (in %) of boric acid $B(OH)_3$ (fine dotted lines) and borate ($B(OH)_4^-$ (coarse dotted lines) in hydrothermal fluids at 100 and 150 °C (black and red lines, respectively) as a function of pH from 4 to 11. (B) Boron isotope composition (‰) of boric acid $B(OH)_3$ (fine dotted lines) and borate ($B(OH)_4^-$ (coarse dotted lines) in hydrothermal fluids and serpentine (continuous lines) at 100 and 150 °C (black and red lines, respectively) as a function of pH from 4 to 11 assuming an initial $\delta^{11}B$ of hydrothermal fluid of +25‰ (blue line). (C) Boron isotope composition (‰) of boric acid $B(OH)_3$ (fine dotted lines) and borate ($B(OH)_4^-$ (coarse dotted lines) in hydrothermal fluid and serpentine (continuous lines) at 100 °C as a function of pH from 4 to 11 assuming an initial $\delta^{11}B$ of hydrothermal fluids of +8‰ (blue line). Green field in (B—C) represents the mean $\delta^{11}B$ signature of samples SG15–4 and ISC13–1, showing negative imprint. Dashed fields in (B—C) highlight the intersection between calculated $\delta^{11}B$ curve for serpentine and pH at different *T*. Neutral pH values at 100 and 150 °C are shown (black and red stars, respectively). Calculations are made using a modified version of the spreadsheet available from Rae (2018); B isotope fractionations between serpentine and borate in fluid are form Cannaò (2020). (For interpretation of the references to colour in this figure legend, the reader is referred to the web version of this article.)

>90% of B in the fluid phase is trigonally coordinated (Fig. 10A; black lines). Assuming a $\delta^{11}B$ signature of +25‰ for the vent fluids and suitable serpentine/fluid B isotope fractionation factors (Cannaò, 2020, and references therein), pH conditions only slightly higher than the neutrality (~ 6.7) can impart negative $\delta^{11}B$ values (down to −6‰) to serpentines (Fig. 10B; shaded field). By considering the $\delta^{11}B$ value of +25‰ for the hydrothermal fluid and higher *T* (150 °C), serpentine minerals reach the $\delta^{11}B$ value of −6‰ at significantly more acid conditions than those modeled at 100 °C. Estimated pH values are from 4.8 to 5.7 (red lines in Fig. 10B), which closely correspond to those measured in the Von Damn hydrothermal vent on ultramafic bedrock at *T* between 100 and 150 °C (McDermott, 2015; Supplementary Fig. 4). Interestingly, these slightly acidic conditions align with the proposed evolution of the N. Apennine system from a high-*T* to a low-*T* hydrothermal vent systems, as suggested to occur at different scales within this ophiolite complex by Alt et al. (2018) and Schwarzenbach et al. (2018). If a $\delta^{11}B$ value of +8‰ for the hydrothermal fluids and *T* of 100 °C are considered, the modelling indicates that serpentine minerals will acquire $\delta^{11}B$ values of −6‰ at pH condition of ~8.7, which is significantly higher than the pH neutrality of *ca.* 2.5 (Fig. 10C). Determining the most representative model between those proposed is challenging without further knowledge on the B isotope behaviour in present-day hydrothermal systems.

The $\delta^{11}B$ results presented in this study highlight the significance of hydrothermal systems in producing altered ultramafic rocks with highly heterogeneous B isotopic signatures. This raises important questions about the process(es) responsible for modifying the $\delta^{11}B$ values of ophicarbonates, which warrant further detailed investigations. So far, serpentines with low (<+10‰) and negative $\delta^{11}B$ signatures have typically been associated to wedge-derived serpentinites flushed by deep slab-derived and ^{11}B-poor fluids, rather than be a signature from oceanic settings (Martin et al., 2016). Therefore, understanding the process(es) responsible for the negative $\delta^{11}B$ imprint shown in the oceanic ophicarbonates from our study is essential to comprehend the B isotope contribution of ophicarbonates in subduction zone settings and to further discern the derivation of serpentinites in ophiolitic terranes.

5.3. Implications for B and C cycles in subduction zones

The dehydration of serpentinized ultramafic rocks in subduction zones represents a major episode of fluid release at sub-arc depths (Scambelluri et al., 2019, and references therein). The distribution of chemical components between subducted dehydrated metaperidotites and fluids is a critical process that controls the recycling of volatile and incompatible elements in the Earth's mantle and contributes to the development of geochemical heterogeneities (Cannaò et al., 2023, 2020b; Scambelluri et al., 2015). Both models and natural observations have demonstrated that the B isotope composition of metamorphic olivine formed after antigorite breakdown under closed-system conditions is ^{11}B-enriched (Cannaò, 2020; Clarke et al., 2020). This enrichment is mainly related to the strong B isotope fractionation in response to the change in B-coordination from antigorite to olivine (tetragonal *vs.* trigonal, respectively; Ingrin et al., 2014). Moreover, the subduction fluids released by deserpentinization are expected to be enriched in $\delta^{11}B$ compared to the newly formed olivine (Cannaò, 2020). Considering the lowest $\delta^{11}B$ signatures of *ca.* -6‰ documented in our ophicarbonates (Table 1, Fig. 4), the partial to complete dehydration of serpentine at increasing *P* should promote the crystallization of metamorphic olivine with $\delta^{11}B$ of +1 to −2‰ in equilibrium with fluids exhibiting B isotope signatures between +6 and + 2‰. This finding shifts to lower $\delta^{11}B$ values the B isotope imprint of serpentine-derived fluids often invoked to explain ^{11}B-rich minerals in both metamorphic terranes (*e.g.*, Halama et al., 2020) or in volcanic arcs (Tonarini et al., 2011).

The dissolution of carbonate in aqueous fluids is a boost for C mobilization in subduction settings (Ague and Nicolescu, 2014), and it also has implications for the long-term global C cycle (Plank and Manning, 2019). Despite the large release of H_2O during antigorite breakdown, thermodynamic modelling indicates that the total CO_2 loss during internally-derived fluid percolation is limited (Menzel et al., 2020). This allows carbonate phases to be recycled deep into the mantle (Eberhard et al., 2023; Menzel et al., 2020). In contrast, the infiltration of external fluids resulting from the devolatilization of serpentinites underlying ophicarbonates present an intriguing scenario for mobilizing C in subduction zones (Menzel et al., 2020; Scambelluri et al., 2016). According to modeling (Menzel et al., 2020), the progressive dissolution of carbonates induced by the infiltration of such fluids will lead to an increasing loss of C as $CO_{2\ aq}$ and C-bearing complex species (*e.g.,* $CaHCO_{3aq}^{-}$, $HCO_{3\ aq}^{-}$) with the consequent formation of new metamorphic olivine and diopside. Considering that B concentration in carbonates from oceanic ophicarbonates is generally low (< 1 ppm; Cannaò et al., 2020a), the B isotopic signature of the newly formed silicates (olivine and diopside) will mostly reflect the composition of the external fluid source. This process will result in carbonate-bearing metaperidotites with at least two generations of metamorphic olivine/diopside with different $\delta^{11}B$ values: the first generation related to the antigorite destabilization, and the second generation related to the carbonate dissolution process(es). The latter is expected to be enriched in [B] and $\delta^{11}B$ compared with the former one, as the fluids triggering carbonate dissolution should be sourced from unmodified oceanic serpentinites (*i.e.,* ^{11}B-enriched composition). Similarly, metamorphic diopside formed either by reaction with $SiO_{2,aq}$ at low (aCO_2) (Debret et al., 2018; Scambelluri et al., 2016) or by the direct reaction between serpentine and $CaCO_3$ (Eberhard et al., 2023) may store B in trigonal coordination (Hålenius et al., 2010), making it isotopically heavier compared to, for instance, clinopyroxenes from mélange terranes often characterized by negative $\delta^{11}B$ imprints (Martin et al., 2016). We speculate that B isotope composition of metamorphic olivine and diopside in such lithologies has the potential to provide key information to unravel carbonate dissolution processes in high-*P* rocks.

While the proposed scenario requires further identification in the natural rock record and experimental investigation, the evidence discussed in this study underscores the significance of ophicarbonates subduction as a crucial mechanism for introducing heterogeneous $\delta^{11}B$ reservoirs to depth and to generate B- and C-bearing fluids at high-*P*. These geochemical features have the potential to hold important implications for the B and C cycles in the Earth's system since the onset of modern plate tectonics. By understanding the processes involved in ophicarbonate subduction and their effects on B and C isotopic compositions, we can gain valuable insights into the recycling of these elements within the Earth's mantle and their influence on global geochemical cycles. Further research in this area will contribute to a deeper understanding of subduction zone processes and their impact on the Earth's chemical evolution.

6. Conclusions

In this contribution we report, for the first time, the *in-situ* B isotope composition of serpentine from ophicarbonates through LA-MC-ICP-MS. This novel approach provides valuable new insights into the variations and controls on the physical-chemical conditions of fluid-rock interaction during progressive evolution of long-lived fossil ultramafic-hosted hydrothermal system. Remarkably, we report the first occurrence of negative $\delta^{11}B$ imprints in serpentine from oceanic environment discussing their relationship with hydrothermal processes and the potential inheritance from precursor serpentinites. Resting also on the conclusions drawn by previous works, we discussed how subduction processes can modify the geochemistry of ophicarbonates and the information that can be gather by studying B isotopes in these lithologies. Finally, we speculated that the deep subduction of ophicarbonates has the potential to endow metaperidotites (*i.e.,* de-carbonated and de-serpentinized rocks) with heterogeneous $\delta^{11}B$ imprints. Such imprints are of great significance in understanding the B- and C-cycles within the Earth's mantle

throughout its history since the inception of modern plate tectonics.

Supplementary data to this article can be found online at https://doi.org/10.1016/j.chemgeo.2023.121899.

Declaration of Competing Interest

The authors declare that they have no known competing financial interests or personal relationships that could have appeared to influence the work reported in this paper.

Data availability

Data will be made available on request.

Acknowledgments

This work benefit funding from the Italian Ministry of University and Research (MUR) – Excellent Departments Projects. EC acknowledges the Società Italiana di Mineralogia e Petrologia (SIMP) for the support through the Research Grant "Fiorenzo Mazzi" for the year 2022. Gianluca Sessa is warmly acknowledged for support during the micro-analytical sessions. EC and MT thanks Guillong M. and Roberts N. for providing the U—Pb calcite reference materials. Cees-Jan De Hoog is warmly thanked for providing the reference Koh-OL olivine. We thank Esther Schwarzenbach and an anonymous referee for reviews and comments, and Don Porcelli for careful editorial handling. We express our gratitude to the University of Milan for covering the open access publishing fee under the CARE-CRUI agreement.

References

Agostini, S., di Giuseppe, P., Manetti, P., Doglioni, C., Conticelli, S., 2021. A heterogeneous subcontinental mantle under the African–Arabian Plate boundary revealed by boron and radiogenic isotopes. Sci. Rep. 11 https://doi.org/10.1038/s41598-021-90275-7.

Ague, J.J., Nicolescu, S., 2014. Carbon dioxide released from subduction zones by fluid-mediated reactions. Nat. Geosci. 7, 355–360. https://doi.org/10.1038/ngeo2143.

Alt, J., Crispini, L., Gaggero, L., Levine, D., Lavagnino, G., Shanks, P., Gulbransen, C., 2018. Normal faulting and evolution of fluid discharge in a Jurassic seafloor ultramafic-hosted hydrothermal system. Geology 46, 523–526. https://doi.org/10.1130/G40287.1.

Alt, J.C., Garrido, C.J., Shanks, W.C., Turchyn, A., Padrón-Navarta, J.A., López Sánchez-Vizcaíno, V., Gómez Pugnaire, M.T., Marchesi, C., 2012a. Recycling of water, carbon, and sulfur during subduction of serpentinites: a stable isotope study of Cerro del Almirez, Spain. Earth Planet. Sci. Lett. 327–328, 50–60. https://doi.org/10.1016/j.epsl.2012.01.029.

Alt, J.C., Shanks, W.C., Crispini, L., Gaggero, L., Schwarzenbach, E.M., Früh-Green, G.L., Bernasconi, S.M., 2012b. Uptake of carbon and sulfur during seafloor serpentinization and the effects of subduction metamorphism in Ligurian peridotites. Chem. Geol. 322–323, 268–277. https://doi.org/10.1016/j.chemgeo.2012.07.009.

Andreani, M., Escartin, J., Delacour, A., Ildefonse, B., Godard, M., Dyment, J., Fallick, A. E., Fouquet, Y., 2014. Tectonic structure, lithology, and hydrothermal signature of the rainbow massif (Mid-Atlantic Ridge 36° 14'N). Geochem. Geophys. Geosyst. 15, 3543–3571. https://doi.org/10.1002/2014GC005269.

Barrett, T.J., Friedrichsen, H., 1989. Stable isotopic composition of atypical ophiolites from East Liguria, Italy. Chem. Geol. 80, 71–84.

Benton, L.D., Ryan, J.G., Tera, F., 2001. Boron isotope systematics of slab fluids as inferred from a serpentine seamount, Mariana forearc. Earth Planet. Sci. Lett. 187 (3–4), 273–282.

Borsi, L., Schiirer, U., Gaggero, L., Crispini, L., 1996. Age, origin and geodynamic significance of plagiogranites in lherzolites and gabbros of the Piedmont-Ligurian Ocean basin. Earth Planet. Sci. Lett. 140, 227–241.

Boschi, C., Dini, A., Früh-Green, G.L., Kelley, D.S., 2008. Isotopic and element exchange during serpentinization and metasomatism at the Atlantis Massif (MAR 30°N): Insights from B and Sr isotope data. Geochim. Cosmochim. Acta 72, 1801–1823. https://doi.org/10.1016/j.gca.2008.01.013.

Cannaò, E., 2020. Boron isotope fractionation in subducted serpentinites: a modelling attempt. Lithos 376–377. https://doi.org/10.1016/j.lithos.2020.105768.

Cannaò, E., Scambelluri, M., Bebout, G.E., Agostini, S., Pettke, T., Godard, M., Crispini, L., 2020a. Ophicarbonate evolution from seafloor to subduction and implications for deep-Earth C cycling. Chem. Geol. 546 https://doi.org/10.1016/j.chemgeo.2020.119626.

Cannaò, E., Tiepolo, M., Bebout, G.E., Scambelluri, M., 2020b. Into the deep and beyond: Carbon and nitrogen subduction recycling in secondary peridotites. Earth Planet. Sci. Lett. 543 https://doi.org/10.1016/j.epsl.2020.116328.

Cannaò, E., Milani, S., Merlini, M., Tiepolo, M., Fumagalli, P., 2023. Phase-a as boron carrier in the Earth's interior. Lithos. https://doi.org/10.1016/j.lithos.2023.107211.

Catanzaro, E.J., Champion, C.E., Garner, E.L., Marinenko, G., Sappenfield, K.M., Shields, W.R., 1970. Boric acid: isotopic and assay standard reference materials. Nat. Bureau Stand. Inst. Mater. Res. 260, 1–70.

Clarke, E., de Hoog, J.C.M., Kirstein, L.A., Harvey, J., Debret, B., 2020. Metamorphic olivine records external fluid infiltration during serpentinite dehydration. Geochem. Perspect. Lett. 16, 25–29. https://doi.org/10.7185/GEOCHEMLET.2039.

Coltat, R., Branquet, Y., Gautier, P., Campos Rodriguez, H., Poujol, M., Pelleter, E., McClenaghan, S., Manatschal, G., Boulvais, P., 2019. Unravelling the root zone of ultramafic-hosted black smokers-like hydrothermalism from an Alpine analog. Terra Nova 31, 549–561. https://doi.org/10.1111/ter.12427.

Cortesogno, L., Gianelli, G., Piccardo, G., 1975. Preorogenic metamorphic and tectonic evolution of the ophiolite mafic rocks (Northern Apennine and Tuscany). Ital. J. Geosci. 94, 291–327.

Cortesogno, L., Galbiati, B., Principi, G., 1980. Le brecce serpentinitiche giurassiche della Liguria orientale. Arch. Sci. Genève 33, 185–200.

Debret, B., Bouilhol, P., Pons, M.L., Williams, H., 2018. Carbonate transfer during the onset of slab devolatilization: New insights from fe and Zn stable isotopes. J. Petrol. 59, 1145–1166. https://doi.org/10.1093/petrology/egy057.

Decitre, S., Deloule, E., Reisberg, L., James, R., Agrinier, P., Mével, C., 2002. Behavior of Li and its isotopes during serpentinization of oceanic peridotites. Geochem. Geophys. Geosystems. 3 (1), 1–20. ISO 690.

Diehl, A., Bach, W., 2020. MARHYS (MARine HYdrothermal Solutions) Database: a Global Compilation of Marine Hydrothermal Vent Fluid, End Member, and Seawater Compositions. Geochem. Geophys. Geosyst. 21 https://doi.org/10.1029/2020GC009385.

Dodd, M.S., Papineau, D., Grenne, T., Slack, J.F., Rittner, M., Pirajno, F., O'Neil, J., Little, C.T.S., 2017. Evidence for early life in Earth's oldest hydrothermal vent precipitates. Nature 543, 60–64. https://doi.org/10.1038/nature21377.

Douville, E., Charlou, J.L., Oelkers, E.H., Bienvenu, P., Colon, C.F.J., Donval, J.P., Fouquet, Y., Prieur, D., Appriou, P., 2002. The rainbow vent fluids (36°14VN, MAR): the influence of ultramafic rocks and phase separation on trace metal content in Mid-Atlantic Ridge hydrothermal fluids. Chem. Geol. 184, 38–48.

Eberhard, L., Plümper, O., Frost, D.J., 2023. Early release of H2O during subduction of carbonated ultramafic lithologies. Contrib. Mineral. Petrol. 178, 17. https://doi.org/10.1007/s00410-023-01997-y.

Foustoukos, D.I., Savov, I.P., Janecky, D.R., 2008. Chemical and isotopic constraints on water/rock interactions at the lost City hydrothermal field, 30°N Mid-Atlantic Ridge. Geochim. Cosmochim. Acta 72, 5457–5474. https://doi.org/10.1016/j.gca.2008.07.035.

Halama, R., Konrad-Schmolke, M., de Hoog, J.C.M., 2020. Boron isotope record of peak metamorphic ultrahigh-pressure and retrograde fluid–rock interaction in white mica (Lago di Cignana, Western Alps). Contrib. Mineral. Petrol. 175 https://doi.org/10.1007/s00410-020-1661-8.

Hålenius, U., Skogby, H., Edén, M., Nazzareni, S., Kristiansson, P., Resmark, J., 2010. Coordination of boron in nominally boron-free rock forming silicates: evidence for incorporation of BO3 groups in clinopyroxene. Geochim. Cosmochim. Acta 74, 5672–5679. https://doi.org/10.1016/j.gca.2010.06.033.

Ingrin, J., Kovács, I., Deloule, E., Balan, E., Blanchard, M., Kohn, S.C., Hermann, J., 2014. Identification of hydrogen defects linked to boron substitution in synthetic forsterite and natural olivine. Am. Mineral. 99, 2138–2141. https://doi.org/10.2138/am-2014-5049.

Kendrick, M.A., Honda, M., Pettke, T., Scambelluri, M., Phillips, D., Giuliani, A., 2013. Subduction zone fluxes of halogens and noble gases in seafloor and forearc serpentinites. Earth Planet. Sci. Lett. 365, 86–96. https://doi.org/10.1016/j.epsl.2013.01.006.

Kendrick, M.A., Plümper, O., Zhao, J.X., Feng, Y., Defliese, W.F., Müller, I.A., Ziegler, M., 2022. Exhumation and carbonation of the Atlantis Bank core complex constrained by in situ U-Pb dating and Δ47 thermometry of calcite veins, SW Indian Ridge. Earth Planet. Sci. Lett. 584 https://doi.org/10.1016/j.epsl.2022.117474.

Kopf, A., Deyhle, A., Zuleger, E., 2000. Evidence for deep fluid circulation and gas hydrate dissociation using boron and boron isotopes of pore fluids in forearc sediments from Costa Rica (ODP Leg 170). Mar. Geol. 167, 1–28.

Lafay, R., Montes-Hernandez, G., Janots, E., Munoz, M., Auzende, A.L., Gehin, A., Chiriac, R., Proux, O., 2016. Experimental investigation of as, Sb and Cs behavior during olivine serpentinization in hydrothermal alkaline systems. Geochim. Cosmochim. Acta 179, 177–202. https://doi.org/10.1016/j.gca.2016.02.014.

Lafay, R., Baumgartner, L.P., Stephane, S., Suzanne, P., German, M.H., Torsten, V., 2017. Petrologic and stable isotopic studies of a fossil hydrothermal system in ultramafic environment (Chenaillet ophicalcites, Western Alps, France): processes of carbonate cementation. Lithos 294–295, 319–338. https://doi.org/10.1016/j.lithos.2017.10.006.

Lemoine, M., Tricart, P., Boillot, G., 1987. Ultramafic and gabbroic ocean floor of the Ligurian Tethys (Alps, Corsica, Apennines): in search of a genetic imodel. Geology 15, 622. https://doi.org/10.1130/0091-7613(1987)15<622:UAGOFO>2.0.CO;2.

Marschall, H.R., 2018. Boron Isotopes in the ocean floor realm and the mantle. In: Advances in Isotope Geochemistry. Springer, pp. 189–215. https://doi.org/10.1007/978-3-319-64666-4_8.

Martin, C., Flores, K.E., Harlow, G.E., 2016. Boron isotopic discrimination for subduction-related serpentinites. Geology 44, 899–902. https://doi.org/10.1130/G38102.1.

Martin, W., Baross, J., Kelley, D., Russell, M.J., 2008. Hydrothermal vents and the origin of life. Nat. Rev. Microbiol. 6, 805–814. https://doi.org/10.1038/nrmicro1991.

McArthur, J.M., Howarth, R.J., Bailey, T.R., 2001. Strontium Isotope Stratigraphy: LOWESS Version 3: best Fit to the Marine Sr-Isotope Curve for 0-509 Ma and Accompanying Look-up Table for Deriving Numerical Age. J. Geol. 109 (2), 155–170.

McDermott, J.M., 2015. Geochemistry of Deep-Sea Hydrothermal Vent Fluids from the Mid-Cayman Rise, Caribbean Sea (PhD thesis). Chemical Oceanography, MIT/WHOI Joint Program in Oceanography.
McDonough, W.F., Sun, S.S., 1995. The composition of the Earth. Chem. Geol. 120, 223–253.
Menzel, M.D., Garrido, C.J., López Sánchez-Vizcaíno, V., 2020. Fluid-mediated carbon release from serpentinite-hosted carbonates during dehydration of antigorite-serpentinite in subduction zones. Earth Planet. Sci. Lett. 531 https://doi.org/10.1016/j.epsl.2019.115964.
Mével, C., 2003. Serpentinization of abyssal peridotites at mid-ocean ridges. Compt. Rendus Geosci. 335, 825–852. https://doi.org/10.1016/j.crte.2003.08.006.
Perilli, N., Nannini, D., 1997. Calcareous nannofossil biostratigraphy of the Calpionella Limestone and Palombini Shale (Bracco/Val Graveglia unit) in the Eastern Ligurian Apennines (Italy). Ofioliti 22, 213–225.
Petriglieri, J.R., Salvioli-Mariani, E., Mantovani, L., Tribaudino, M., Lottici, P.P., Laporte-Magoni, C., Bersani, D., 2015. Micro-Raman mapping of the polymorphs of serpentine. J. Raman Spectrosc. 46, 953–958. https://doi.org/10.1002/jrs.4695.
Plank, T., Manning, C.E., 2019. Subducting carbon. Nature. https://doi.org/10.1038/s41586-019-1643-z.
Rae, J.W.B., 2018. Boron Isotopes in Foraminifera: Systematics, Biomineralisation, and CO2 Reconstruction. https://doi.org/10.1007/978-3-319-64666.
Scambelluri, M., Pettke, T., Cannaò, E., 2015. Fluid-related inclusions in Alpine high-pressure peridotite reveal trace element recycling during subduction-zone dehydration of serpentinized mantle (Cima di Gagnone, Swiss Alps). Earth Planet. Sci. Lett. 429 https://doi.org/10.1016/j.epsl.2015.07.060.
Scambelluri, M., Bebout, G.E., Belmonte, D., Gilio, M., Campomenosi, N., Collins, N., Crispini, L., 2016. Carbonation of subduction-zone serpentinite (high-pressure ophicarbonate; Ligurian Western Alps) and implications for the deep carbon cycling. Earth Planet. Sci. Lett. 441, 155–166. https://doi.org/10.1016/j.epsl.2016.02.034.
Scambelluri, M., Cannaò, E., Gilio, M., 2019. The water and fluid-mobile element cycles during serpentinite subduction. A review. Eur. J. Mineral. 31 https://doi.org/10.1127/ejm/2019/0031-2842.
Schwartz, S., Guillot, S., Reynard, B., Lafay, R., Debret, B., Nicollet, C., Lanari, P., Auzende, A.L., 2013. Pressure-temperature estimates of the lizardite/antigorite transition in high pressure serpentinites. Lithos 178, 197–210. https://doi.org/10.1016/j.lithos.2012.11.023.
Schwarzenbach, E.M., Steele-MacInnis, M., 2020. Fluids in submarine mid-ocean ridge hydrothermal settings. Elements 16, 389–394. https://doi.org/10.2138/GSELEMENTS.16.6.389.
Schwarzenbach, E.M., Früh-Green, G.L., Bernasconi, S.M., Alt, J.C., Shanks, W.C., Gaggero, L., Crispini, L., 2012. Sulfur geochemistry of peridotite-hosted hydrothermal systems: comparing the Ligurian ophiolites with oceanic serpentinites. Geochim. Cosmochim. Acta 91, 283–305. https://doi.org/10.1016/j.gca.2012.05.021.
Schwarzenbach, E.M., Früh-Green, G.L., Bernasconi, S.M., Alt, J.C., Plas, A., 2013. Serpentinization and carbon sequestration: a study of two ancient peridotite-hosted hydrothermal systems. Chem. Geol. 351, 115–133. https://doi.org/10.1016/j.chemgeo.2013.05.016.
Schwarzenbach, E.M., Gill, B.C., Johnston, D.T., 2018. Unraveling multiple phases of sulfur cycling during the alteration of ancient ultramafic oceanic lithosphere. Geochim. Cosmochim. Acta 223, 279–299. https://doi.org/10.1016/j.gca.2017.12.006.
Schwarzenbach, E.M., Vogel, M., Früh-Green, G.L., Boschi, C., 2021. Serpentinization, Carbonation, and Metasomatism of Ultramafic Sequences in the Northern Apennine Ophiolite (NW Italy). J. Geophys. Res. Solid Earth 126. https://doi.org/10.1029/2020JB020619.
Seyfried, W.E., Dibble, W.E., 1980. Seawater-peridotite interaction at 300°C and 500 bars: implications for the origin of oceanic serpentinites. Geochim. Cosmochim. Acta 44, 309–321.
Seyfried, W.E., Janecky, D.R., Mottl, M.J., 1984. Alteration of the oceanic crust: implications for geochemical cycles of lithium and boron. Geochim. Cosmochim. Acta 48, 557–569. https://doi.org/10.1016/0016-7037(84)90284-9.
Spivack, A.J., You, C.-F., 1997. Boron isotopic geochemistry of carbonates and pore waters, Ocean Drilling Program Site 851. Earth Planet. Sci. Lett. 152 (1–4), 113–122.
Tonarini, S., Leeman, W.P., Leat, P.T., 2011. Subduction erosion of forearc mantle wedge implicated in the genesis of the South Sandwich Island (SSI) arc: evidence from boron isotope systematics. Earth Planet. Sci. Lett. 301, 275–284. https://doi.org/10.1016/j.epsl.2010.11.008.
Treves, B., Hickmott, D., Vaggelli, G., 1995. Texture and microchemical data of oceanic hydrothermal calcite veins, Northern Apennine ophicalcites. Ofioliti 20, 111–122.
Treves, B.E., Harper, G.D., 1994. Exposure of serpentinites on the ocean floor: sequence of faulting and hydrofracturing in the Northern Apennine ophicalcites. Ofioliti 19, 435–466.
Tribuzio, R., Garzetti, F., Corfu, F., Tiepolo, M., Renna, M.R., 2016. U–Pb zircon geochronology of the Ligurian ophiolites (Northern Apennine, Italy): Implications for continental breakup to slow seafloor spreading. Tectonophysics 666, 220–243.
Trumbull, R.B., Slack, J.F., 2018. Boron Isotopes in the Continental Crust: Granites, Pegmatites, Felsic Volcanic Rocks, and Related Ore Deposits. In: Horst, Marschall, Foster, G. (Eds.), Boron Isotopes: The Fifth Element. Springer International Publishing, Cham, pp. 249–272. https://doi.org/10.1007/978-3-319-64666-4_10.
Vermeesch, P., 2018. IsoplotR: a free and open toolbox for geochronology. Geosci. Front. 9, 1479–1493. https://doi.org/10.1016/j.gsf.2018.04.001.
Vils, F., Tonarini, S., Kalt, A., Seitz, H.M., 2009. Boron, lithium and strontium isotopes as tracers of seawater-serpentinite interaction at Mid-Atlantic ridge, ODP Leg 209. Earth Planet. Sci. Lett. 286, 414–425. https://doi.org/10.1016/j.epsl.2009.07.005.
Waite, J.H., Glein, C.R., Perryman, R.S., Teolis, B.D., Magee, B.A., Miller, G., Grimes, J., Perry, M.E., Miller, K.E., Bouquet, A., Lunine, J.I., Brockwell, T., Bolton, S.J., 2017. Cassini finds molecular hydrogen in the Enceladus plume: evidence for hydrothermal processes. Science 1979 (356), 155–159.
You, C.-F., Chan, L.H., Spivack, A.J., Gieskes, J.M., 1995. Lithium, boron, and their isotopes in sediments and pore waters of Ocean Drilling Program Site 808, Nankai Trough: Implications for fluid expulsion in accretionary prisms. Geology 23, 37–40.